Impacts of New Particle Formation on Aerosol Cloud Condensation Nuclei (CCN) Activity in Shanghai: Case Study

Chunpeng Leng [a], Qun Zhang [a], Jun Tao [b], Hefeng Zhang [c], Deqin Zhang [a], Chen Xu [a], Xiang Li [a], Lingdong Kong [a], Tiantao Cheng [a], Renjian Zhang [d], Xin Yang [a], Jianmin Chen [a], Liping Qiao [e], Shenrong Lou [e], Hongli Wang [e], Changhong Chen [e]

a. Shanghai Key Laboratory of Atmospheric Particle Pollution and Prevention (LAP^3), Fudan-Tyndall Centre, Department of environmental science and engineering, Fudan University, Shanghai 200433, China;
b. South China Institute of Environmental Sciences, Ministry of Environmental Protection, Guangzhou 510655, China;
c. Atmospheric Environment Institute, Chinese Research Academy of Environmental Sciences, Beijing 100012, China;
d. Key Laboratory of Region Climate-Environment Research for Temperate East Asia, Institute of Atmospheric Physics, Chinese Academy of Sciences, Beijing 100029, China;
e. State Environmental Protection Key Laboratory of the Cause and Prevention of Urban Pollution Complex, Shanghai Academy of Environmental Sciences, Shanghai 200233, China;

* Corresponding authors: Tiantao Cheng; Jianmin Chen
Tel: (86) 21-6564 3230; fax: (86) 21-6564 2080;
Email: ttcheng@fudan.edu.cn, jmchen@fudan.edu.cn

Abstract

New particle formation (NPF) events and their impacts on cloud condensation nuclei (CCN) were investigated using continuous measurements collected in urban Shanghai from 1 to 30 April 2012. During the campaign, NPF occurred in 8 out of the 30 days and enhanced CCN number concentration (N_{CCN}) by a factor of 1.2-1.8, depending on supersaturation (SS). The NPF event on 3 April 2012 was chosen as an example to investigate the NPF influence on CCN activity. In this NPF event, secondary aerosols were produced continuously and increased $PM_{2.5}$ mass concentration at a rate of 4.33 μg cm^{-3} h^{-1}, and the growth rate (GR) and formation rate (FR) were on average 5 nm h^{-1} and 0.36 cm^{-3} s^{-1}, respectively. The newly formed particles grew quickly from nucleation mode (10-20 nm) into CCN size range. N_{CCN} increased rapidly at SS of 0.4-1.0% but weakly at SS of 0.2%. Correspondingly, aerosol CCN activities (fractions of activated aerosol particles in total aerosols, N_{CCN}/N_{CN}) were significantly enhanced from 0.24-0.60 to 0.30-0.91 at SS of 0.2-1.0% due to the NPF. On the basis of the κ-Köhler theory, aerosol size distributions and chemical composition measured simultaneously were used to predict N_{CCN}. There was a good agreement between the predicted and measured N_{CCN} (R^2=0.96, $N_{predicted}/N_{measured}$=1.04). This study reveals that NPF exerts large impacts on aerosol particle abundance and size spectra, thus significantly promotes N_{CCN} and aerosol CCN

activity in this urban environment. The GR of NPF is the key factor controlling the newly formed particles to become CCN at all SS levels, whereas the FR is an effective factor only under high SS (e.g. 1.0%) conditions.

1. Introduction

Atmospheric aerosols exert great impacts on global climate by affecting the earth's radiation balance through directly scattering and absorbing solar and terrestrial lights, and indirectly modifying cloud by acting as cloud condensation nuclei (CCN) (Charlson et al., 1992; Lohmann et al., 2005). The indirect effect of primary and secondary aerosols brings up the largest uncertainty to predictions of aerosol radiative forcing and global climate change (IPCC, 2013). So far, many studies of field observation and modeling have found that new particle formation (NPF) significantly impacts aerosols and CCNs at worldwide locations (Ghan et al., 2001; Spracklen et al., 2006, 2008; Zhang, 2010).

Normally, NPF in the atmosphere is identified as the nucleation of gas phase precursors and subsequent condensational growth, which is a crucial secondary transformation course (Birmili et al., 2000; Kulmala et al., 2004). In fact, NPF consists of a complex set of procedures, including the formation of nanometer-size clusters from gaseous vapors, the growth of these clusters, the removal of growing clusters by coagulation with

pre-existing particles, and the further growth of survived clusters into aerosol particles, some of which are large enough to become CCN (McMurry et al., 1983, 2005； Weber et al., 1996). The NPF event can be effectively characterized by the formation rate (FR) of nucleation mode particles and the growth rate (GR) of freshly nucleated particles (Kulmala et al., 2012). On the basis of over 100 field measurements summarized by Wang et al. (2013), significant gaps still exist regarding both formation and growth rate outputs. For example, the GR varied in the range of 1-20 nm h^{-1} and the FR in 0.01-10 cm^{-3} s^{-1}. Condensable gaseous precursors and their coagulation sink responsible for NPF are commonly high in megacities of developing countries (Mönkkönen et al., 2005; Wu et al., 2007). Gaseous sulfur is proved to play a vital role in nucleation process (Petäjä et al., 2009; Kulmala et al., 2013). Atmospheric ammonia can effectively lower the surface pressure of gaseous sulfuric molecular and participates homogeneous nucleation with gaseous sulfuric acid and water vapor (Smith et al., 2004; Sakurai et al., 2005; Gaydos et al., 2005). In addition, there are other species responsible for NPF such as amines (Yu et al., 2012; Benson et al., 2011), low-volatile organic vapors (Metzger et al., 2010; Paasonen et al., 2010; Riipinen et al., 2011; Ehn et al., 2014) and iodine compounds (O'Dowd et al., 2002; Vuollekoski et al., 2009).

The newly formed particles from atmospheric nucleation are often able to grow into CCN size and further influence cloud properties or even

global climate (Kerminen et al., 2005; Laaksonen et al., 2005; Wiedensohler et al., 2009). Kerminen et al. (2012) presents a synthesis of our current (by the end of 2012) knowledge of CCN production associated with atmospheric nucleation, and concludes that CCN production associated with atmospheric nucleation is both frequent and widespread phenomenon in numerous types of continental boundary layers, and probably also for a large fraction of the free troposphere. The latest model results show that the NPF events contribute much more to global aerosol number burden than primary emissions (Merikanto et al., 2009; Yu et al., 2008). Under numerous atmospheric conditions aerosol has a positive feedback to CCN number concentration (N_{CCN}) (Ramanathan et al., 2001; Laaksonen et al., 2005), and N_{CCN} usually exhibits a significant increase after NPF (O'Dowd et al., 2001; Lihavainen et al., 2003; Kuwata et al., 2008; Yue et al., 2011). Due to various chemical species involved in NPF, the extent of NPF effects on CCN varied temporarily and spatially (Spracklen et al., 2008; Pierce and Adams, 2009). The long-term NPF observations were mainly conducted in Europe and North America, whereas little has been done in developing countries (Wang et al., 2013). To date, only a few studies have concerned NPF and its interaction with CCN in China. Yue et al. (2011) reported that the GR of sulfur-poor NPF was on average about 80% larger than that of sulfur-rich NPF, and the NPF events increased CCN by 0.4-6

times in Beijing, where various source apportionment of $PM_{2.5}$ was reported by Zhang et al. (2013). Wiedensohler et al. (2009) found that the CCN size distribution is dominated by the growing nucleation mode in Beijing, which accounted up to 80% of the total CCN number concentration, in contrast to the usually found phenomenon of the dominance by the accumulation mode.

In the present study, we analyze a comprehensive dataset of 1-month simultaneous measurements of aerosol size spectra, N_{CCN}, black carbon (BC), water-soluble ions and gaseous pollutants to understand the NPF events and their impacts on N_{CCN} and aerosol CCN activity in an urban environment of Shanghai, one of the largest cities in China. A closure study between predicted and measured CCNs is also conducted to investigate the influence of aerosol chemical composition on its growth to CCN. An effective CCN prediction model is further developed based on model-measurement comparison results.

2. Experimental

2.1 Observational site

All instruments were mounted on the roof of one building approximately 20m above the ground in the campus of Fudan University (31˚18′N, 121˚29′E) located in Shanghai. The observational site is mainly surrounded by urban residential areas, where no large local emission was detected during this study. The East China Sea is

approximate 40 km east of the site. Except CCN, other measurements conducted synchronously, including aerosol number size distribution (condensation nuclei (CN) of 10-800 nm), major inorganic water-soluble ions in aerosol particles, gaseous pollutants and meteorological factors. Local time (LT) used in this study is eight hours ahead of UTC.

2.2 Measurement and instrumentation

A CCN counter (CCN-100, DMT, USA) with continuous flow and single column (Roberts and Nenes, 2006; Lance et al., 2006) was employed to monitor CCN concentrations at supersaturated conditions (SS in the range of 0.07-2%). Before the campaign, the instrument was calibrated for SS using standard $(NH_4)_2SO_4$ particles. To maintain stable SS, according to the instrument operation manual, regular calibrations were also performed for temperature gradient, input and shear airflows and pressure (Leng et al., 2013). In addition, periodic zero checks were done to ensure counting accuracy for optical particle counter (OPC) installed inside the CCN counter. The ambient aerosol was firstly dried by a dryer (active carbon) to lower relative humidity (RH) below 30%, and subsequently introduced into the CCN counter (Leng et al., 2013).

Aerosol particle size distributions in the size range of 10-800 nm were measured using a high-resolution scanning mobility particle sizer (SMPS, TSI 3080, USA). Before and after the field campaign, the instrument was calibrated to maintain accurate particle sizing. The SMPS data are

recorded by AIM (Aerosol Instrument Management) software from TSI company. The SMPS 3936 (TSI corp.) is employed to track the size distribution change, in which the CPC 3736 (TSI corp.) is used to count the number of particle of each size. The neutralizer 3077a (TSI corp.) is used in the system to provide known charge on the particles going into the SMPS. The size of the employed impactor is 0.071 cm. Both multiple charge and the diffusion correction is applied. The inlet information has been reported in our previously papers (Wang et al., 2009; Huang et al., 2013).

BC was measured by an online monitor of Aethalometer (AE-31, Magee Scientific Co., Berkeley, California, USA) at a 5-min time resolution and a 5 l/min airflow rate. According to the strong ability of BC light absorption at near infrared wavelengths (Hansen et al., 1984; Weingartner et al., 2003), BC mass is determined using the light attenuation at 880 nm and the appropriate specific attenuation cross section proportional to BC (Petzold et al., 1997). The attenuation can be calculated based on the intensity difference of reference and sensing beams between light on and off (Dumka et al., 2010). In order to screen the impacts of other absorptive material, the data contaminated by mineral and dust aerosols were excluded from BC measurements. Details for instrument operating and calibrating can be found in Cheng et al. (2010).

A monitor of aerosols and gases (MARGA, ADI 2080, Netherlands) was employed to measure the mass concentrations of major inorganic water-soluble ions (Na+, K^+, Mg^+, Ca^+, SO_4^{2-}, Cl^-, NO_3^- and NH_4^+) in ambient aerosol particles at a 1h time resolution. The methods of sampling, operation and internal calibration of the MARGA were described in Du et al. (2011).

A continuous ambient particulate monitor (FH62C14, Thermo) was used to measure $PM_{2.5}$ (particles in aerodynamic diameter less than 2.5 μm) concentration online. The Thermo FH62C14 Continuous Ambient Particulate Monitor (FH62C14) is a radiometric particulate mass monitor capable of providing real-time measurements. It incorporates time-averaged measurements of an integral beta attenuation sensor and advanced firmware to optimize the continuous mass measurement. The FH62C14 equips a dynamic heating system (DHS) to maintain the relative humidity (RH) of the air passing through the filter tape of the radiometric stage well below the point at which the collected particles accrete and retain liquid water. The DHS system minimizes the internal temperature rise ensuring negligible loss of semi-volatiles from the collected sample when the ambient RH is below the threshold to which the heater is controlling. As the ambient RH increases above the threshold, the applied heating is optimized to maintain the RH threshold above the beta attenuation filter tape. Necessary sensor calibrations are performed

for temperature, relative humidity, barometric pressure and volumetric flow regularly to maintain valid measurements.

Moreover, an automatic weather station client (HydroMet^{TM}, Vaisala) and a visibility monitor (Belford, M6000) were employed to collect the data of meteorological variables and atmospheric visibility.

3. Results and discussion

3.1 Overview of the entire period

The ground-based measurements contained N_{CCN} at SS of 0.2-1.0%, aerosol size spectra, atmospheric visibility, $PM_{2.5}$, BC, aerosol inorganic water-soluble ions and SO_2 and were conducted during the period of 1-30 April 2012. Figure 1 describes the general meteorological conditions (e.g. wind speed, wind direction, RH and temperature) for the entire period. Wind frequently changed direction and were mostly weaker than 6 m s^{-1}. There was no significant precipitation in this month and RH seldom exceeded 90%. Temperature generally varied between 10-25 ℃.

Figure 2 shows the temporal variations of 5-min mean SO_2, $PM_{2.5}$ concentration and atmospheric visibility for the entire period. In general, $PM_{2.5}$ and visibility were negatively correlated and averaged 70±60 μg m^{-3} and 24.3±23.7 km, respectively. The maximum and average of $PM_{2.5}$ in the current study is of less magnitude than those measured in a previous study in 2006 in this urban environment which showed a range of 17.8-217.9 μg m^{-3} and an average of 94.6 μg m^{-3} (Wang et al., 2006).

$PM_{2.5}$ frequently experienced a clear inter-day oscillating with a similar intra-day cycle. $PM_{2.5}$ can reflect the variations of ambient particulate pollutant loadings in the boundary atmosphere layer, and can be viewed as an additional proxy of pre-existing particle amounts for identifying NPF. In a broad view, atmospheric visibility frequently declined to be less than 10 km, revealing heavily polluted episode occurrences (e.g. haze). In fact, the haze or hazy days accounted for 50% of the study period, during which atmospheric visibility was on average 5.65 km, while it was 24.3 km on average for the rest of the days.

3.1.1 New particle formation events

It has been widely accepted that the key criterion for discerning an NPF event is to identify an acute burst of nucleation mode particles, known as newly formed particles up to detectable size of 3 nm exceeding the background level and lasting for several hours and subsequent growth in mean particle size (Birmili and Wiedensohler, 2000; Kulmala et al., 2004, 2012; Vakkari et al., 2011). The supplementary criterions are also needed for identifying NPF, such as low pre-existing particle loading, an apparent “banana” shaped particle number concentration as a function of time and size, and favorable weather conditions essential for excluding pre-existing particle disturbance particularly in urban environment (Shi et al., 2001; Heintzenberg et al., 2007; Olofson et al., 2009). In this study, although the SMPS is only capable of capturing particles no less than 10

nm, the aerosol size spectra from the SMPS measurements was available to determine NPF and to calculate the FR and GR of NPF.

In this study, the days with distinct bursts of nucleation mode (10-20 nm) particles lasting for at least 1.5 h from their initial outbreak to maximum in number concentration, and with apparent growth to larger sizes (e.g. 20-50 nm) for a few hours, were defined as effective NPF days. The rest of the days were defined as non-NPF days. Figure 3 shows the 1-month series of aerosol size distribution, 4-min mean total (N_{total}) and nucleation mode ($N_{10-20nm}$) aerosol number concentration and 1 h mean CCN concentration. On a whole, 8 out of the 30 days were characterized as the NPF days, which represented an occurrence frequency of 27% and was much higher than the 5.4% measured by Du et al (2012) at the same site in winter. Many studies have observed greater NPF frequency in springtime in northern hemisphere. For example, seasonal NPF pattern with a spring maximum and winter minimum is typical for all Nordic stations (Dal Maso et al., 2007; Kristensson et al., 2008; Vehkamäki et al., 2004). In North China Plain, The number of events was highest in the spring months (Wang et al., 2013). The high frequency during spring in urban Shanghai is probably due to high frequency of strong wind from northern China, which helps removing the pre-existing particles in the atmosphere and further favors the occurrence of new particle formation events (Wu et al., 2008; Wang et al., 2013).

3.1.2 Formation and growth rate, and condensation sink

Formation and growth rates are two essential factors characterizing NPF events (Yue et al., 2011; Kulmala et al., 2012). The FR rate is theoretically defined as the mean increase rate of nucleation mode particle in number concentration as a function of time ($dN_{nucleation}/dt$) during the nucleation stage of a NPF event. In this paper, due to the losses of newly-formed nucleated particles caused by coagulation, and the measurement unavailable for 3-10 nm particles, this calculation only yielded an "apparent particle formation rate (APFR)" (Du et al., 2012). It should be noted that this APFR would be an underestimate in comparison with the actual formation rate. On the other hand, the GR rate refers to the mean size growing rate of nucleated particles in geometric mean diameter as a function of time during the growth stage of a NPF event, which has been described in details elsewhere (Kulmala et al., 2001, 2004b; Dal Masol et al., 2005). The mode diameter, namely a calibrated geometric mean diameter automatically made by SMPS itself for all aerosol size bins instead of only for nucleated particles, is used to calculate particle growth rate in this study. Similarly, this calculation produces an "apparent particle growth rate (APGR)". The APGR would be an overestimate in comparison with the real growth rate due to inclusion of the GR rate caused by coagulation, which is not related to particle mass increases (Kerminen and Kulmala., 2002).

The condensation sink (CS) describes how rapidly vapor molecules can condense onto the particles and can be used to represent the pre-existing particle concentrations (Kulmala et al., 2001). Its values can be directly calculated from the measured aerosol particle size distributions using equation (1) as following:

$$CS = 2\pi D \sum \beta D_p N \quad (1)$$

Where D is the diffusion coefficient of the condensing vapor, β is the transitional regime correction factor and can be determined using method from Fuchs and Sutugin (1971), D_p is the particle diameter and N is the particle number concentration of corresponding size. More explanations and the derivation process for equation (1) can be seen in many studies (Kulmala et al., 2001, 2005; Dal Maso et al., 2002, 2005; Gong et al., 2010; Shen et al., 2011; Gao et al., 2012; Wang et al., 2013), therefore it was only briefly summarized here. It is worth noting that this calculated CS might be underestimated compared to the real values because its derivation is based on the dry particle number size distributions incapable of necessarily representing ambient wet condition well in this study. The uncertainty coming from the effect of ambient hygroscopic growth of aerosols on CS ranges from 5% to 50% (Kulmala et al., 2001).

The mean formation and growth rates of NPF events were 0.40 cm^{-3} s^{-1} and 4.91 nm h^{-1}, respectively, during the whole campaign. The formation and growth rates showed a strong location dependence, for example,

higher formation and growth rates have been observed in New Delhi (3.3-13.9 cm^{-3} s^{-1}, 11.6-18.1 nm h^{-1}) and Atlanta (20-70 cm^{-3} s^{-1}), while comparable values were measured in Beijing (6 cm^{-3} s^{-1}, 4 nm h^{-1}) for sulfur-rich aerosol type and (2 cm^{-3} s^{-1}, 6 nm h^{-1}) for sulfur-poor aerosol type and in Shanghai (3.3-5.5 nm h^{-1}) (Kulmala et al., 2004; Mönkkönen et al., 2005; Yue et al., 2011; Du et al., 2012). The mean CS values were 0.021 s^{-1} on the NPF event days and 0.040 s^{-1} on the non-event days, lower than those measured in Beijing (0.027±0.021 and 0.047±0.024 s-1) and New Delhi (0.050-0.070 s^{-1}), and higher than those observed in Shangdianzi (SDZ, a regional station located in the North China Plain, about 120 km northeast of Beijing, 0.020±0.020 and 0.026±0.018 s^{-1}), and European urban environments including Marseille (0.003-0.015 s^{-1}), Athens (0.006-0.013 s^{-1}) and Helsinki (0.006 s^{-1}) (Kumala et al., 2005; Hussein et al., 2008; Wang et al., 2013).

3.1.3 NPF impacts on aerosol CCN activity

Pierce and Adams (2007) are the first ones that present the full theoretical framework on the efficiency of CCN production resulting from nucleation. To explore the NPF potential influence on CCN, we further examined the impacts of FR and GR rates in NPF events on N_{CCN} and aerosol CCN activity. Table 1 summarizes the N_{CCN} enhancement ratios for different FR and GR levels during the entire campaign.

It has been widely recognized that N_{CCN} is positively correlated to N_{CN}

under various atmospheric conditions (Ramanathan et al., 2001; Laaksonen et al., 2005), and enhancements on N_{CCN} are expected after NPF events (O'Dowd et al., 2001; Kuang et al., 2009; Yue et al., 2011). Theoretically, the high FR rate produces more secondary aerosol particles (i.e. N_{CN}), which may subsequently impact N_{CCN} if new particles grow into greater sizes (Ghan et al., 2001; Spracklen et al., 2006, 2008; Zhang, 2010). In this paper, however, N_{CCN} was insensitive to the FR rate of NPF at SS of 0.2-0.8%, as indicated by the small differences in N_{CCN} enhancement ratios under various FR and SS values. This finding agrees with the results of earlier studies that the nucleation of newly formed particles within the boundary layer poses a minor impact on N_{CCN}. Carslaw et al. (2007) found that N_{CCN} increased only by 12-17% after a two order of magnitude increase of nucleation rate in central Europe. A similar result has been reported in Beijing (Yue et al., 2011). The possible explanation is in two aspects. The first one is due to the two separate and self-governed processes in particle formation and subsequent growth. A high formation rate does not necessarily correspond to a high GR rate since the newly formed particles may not grow into CCN size with insufficient time period. The second one is due to coagulation process between particles which leads to reduced N_{CN} and further lowers N_{CCN} enhancement ratios. In fact, the impact of FR in NPF on N_{CCN} enhancement increased with SS (Table 1). The lower critical dry diameter

under higher SS for a given aerosol particle was probably the main reason. For example, according to the κ-Köhler theory (Köhler., 1936; Petters and Kreidenweis., 2007), pure NaCl particles can act as CCN only at 65 nm under SS 0.2%, while it can be activated at 22 nm under SS 1.0%. Presumably, with the presence of an unrealistic high SS where all nucleation mode particles (10-20 nm) are activated, the formation rate would be one controlling factor.

On the other hand, what controls a newly formed particle to become a CCN is its survival probability whether it has enough time to grow into thermodynamic stable size by competing with the capture and removal of pre-existing particles (Kerminen et al., 2001; Pierce and Adams, 2007; Zhang et al., 2012). Toward to this end, the aerosol GR rate of NPF responsible for this survival probability was observed to exert a valid effect on N_{CCN} enhancement ratios. As was found in this study, the N_{CCN} enhancement ratios at larger GR rate were higher than those at lower GR rate by a factor of 1.06-1.13 depending on SS.

Overall, the N_{CCN} enhancement ratios due to NPF varied as a function of FR and GR rates and SS. In real atmosphere, SS varys from exceeding 1.0% in clean-air stratus cloud to slightly less than 0.1% in polluted conditions (Hudson and Noble, 2014). FR may logically play a vital role in CCN production in the clean-air stratus cloud while exert a minor impact in polluted conditions. GR is invariably the most important factor

in controlling the extent of newly formed particles in becoming CCN during NPF.

3.2 Characteristics of a typical NPF

3.2.1 Increased concentrations of nanoparticles

The NPF event spanning the period from 10:00 LT on 3 April to 4:00 LT on 4 April is analyzed in detail to shed some light on the relationship between NPF and CCN. This NPF event was identified to consist a nucleation stage (10:00-13:00 LT) and a growth (13:00-4:00 LT) stage (Fig. 4).

Before 10:00 LT on 3 April, $PM_{2.5}$ was below 20 μg m^{-3} due to the relatively strong wind speed (e.g. 6 m s^{-1}) favoring pollutant dispersion. BC was less than 1 μg m^{-3} and atmospheric visibility exceeded 30 km (Fig. 5 and 6). Apparently, the pre-existing particles of nucleation mode (10-20 nm) were low (Fig. 7). Newly formed particles increased quickly in just 1.5 hours from the initial outbreak to the maximum concentration of 1800 cm^{-3} (Fig. 7). During the same time period, N_{CN} increased from 15,000 to 25,000 cm^{-3}. The newly formed particles grew in size in the following periods (the growth stage) due to condensation, heterogeneous reactions of chemical compounds and coagulation between particles (Wang et al., 2010). The temporal variations of median, geometric mean and mode diameters for the measured aerosol population are given in Fig. 7. In general, these three diameters were strongly correlated with each

other and increased in size ever since the nucleation burst occurred. During this period, the wind speed was mostly less than 2 m s^{-1}, implying a weak atmospheric dilution of pollutants. $PM_{2.5}$ increased after 17:00 LT on 3 April, showing a significant enhancement from 38 to 86 μg m^{-3}. In addition, BC correlated well with $PM_{2.5}$, and they both reduce atmospheric visibility.

3.2.2 Insights into chemical species involved

Several factors likely determine if a chemical species is to act as nucleation precursor, including its abundance, reactivity and volatility (Zhang et al., 2012). Gaseous H_2SO_4 has been proved to be a key precursor participating in nucleation process due to its low volatility (Petäjä et al., 2009; Kulmala et al., 2013), and a necessary condition for new particle formation is for its molecular concentration exceeding 10^5 cm^{-3} in atmosphere (Weber et al., 1999, Nieminen et al., 2009). The condensation of gaseous H_2SO_4 together with subsequent neutralization with ammonia plays a dominant role in the growth of Aitken mode particles, whereas it exerts little contribution to the growth of particles in accumulation mode (Zheng et al., 2011).

However, direct measurement of sulfuric acid in ambient air is still challenging, appropriate proxies are needed. Petäjä et al. (2009) measured the sulfuric acid and OH concentration in a boreal forest site in Finland and successfully developed three reasonable proxies for sulfuric

acid concentration by using the measured time series as a foundation. Their proxies refer to source (i.e. gaseous SO_2, hydroxyl radical, solar radiation in 280-320 nm range, and global radiation) and sink (i.e. condensation sink) terms, and the simplest one is the radiation times SO_2 divided by condensation sink. In this paper, the source and radiation terms are unavailable, one may plausibly conjecture similar promotion of H_2SO_4 on the basis of its gaseous precursor (e.g. SO_2) evolution (Zhang et al., 2012).

$$SO_2 + OH \xrightarrow{O_2\ H_2O} H_2SO_4$$

The particle nucleation event showed a burst of 10-20 nm particles when SO_2 peaked at 10:00 LT on 3 April, with its mass and molar concentrations exceeding 4.1 μg m^{-3} and 3.8×10^{10} cm^{-3}, respectively (Fig. 8). Afterwards, SO_2 underwent a gradual decrease down to 1.5 μg m^{-3}, and SO_4^{2-} correspondingly increased from 8 to 10 μg m^{-3}. The good agreement between SO_2 and nucleation mode particles denotes the key role of gaseous sulfur in controlling particle nucleation (Zhang et al., 2012; Kulmala et al., 2013).

Besides gaseous sulfur, other nucleation precursors have been proposed to involve in the critical nucleus formation in numerous environment conditions (Riipinen et al., 2011; Zhang et al, 2012). For example, atmospheric ammonia can significantly lower the surface vapor pressure of gaseous sulfuric acid molecular and participate homogeneous

446 nucleation with gaseous sulfur acid and water vapor. According to the
447 classical ternary homogeneous theory developed recently, the presence of
448 ammonia in ppt level significantly enhances nucleation rates (Yu et al.,
449 2006). Many field measurements and laboratory simulations have
450 corroborated the crucial role of ammonia in the growth of newly formed
451 particles (Smith et al., 2004; Sakurai et al., 2005; Gaydos et al., 2005).
452 Though experimental evidence seems very limited, nitrate has been
453 reported as a crucial contributor to nanoparticle growth, especially for
454 10-30 nm particles where nitrate is dominant (Hildebrandt et al., 2012).
455 Riipinen et al. (2011) combined observations from two continental sites
456 to show that condensation of organic vapors (i.e. non-volatile and
457 semi-volatile species) is a crucial factor governing the lifetimes and
458 climatic importance of the smallest atmospheric particles. Ehn et al.
459 (2014) find that several biogenic VOCs (e.g. monoterpenes) form large
460 amounts of extremely low-volatility vapours and further demonstrate that
461 these low-volatility vapours can enhance (or even dominate) the
462 formation and growth of aerosol particles over forested regions. In this
463 paper, NO_3^- increased by a factor of 1.33 and NH_4^+ increased by a factor
464 of 1.45 during the case NPF event, indicating that the particle growth is
465 partly driven by the condensation of atmospheric precursors (Fig. 8).

466 **3.2.3 Aerosol CCN activity enhancement**

467 Figure 9 shows the temporal evolutions of N_{CCN} and aerosol CCN

activity at SS of 0.2-1.0% for the entire period. The enhanced N_{CN} and reduced aerosol CCN activity, associated with nucleation mode particle burst, was observed between 10:00 and 13:00 LT on 3 April. In contrast to N_{CN} which increased immediately after the burst of nucleation mode particles, there was a 4 h delay in the increase of N_{CCN}. As the newly formed particles grew into larger sizes, both N_{CCN} and aerosol CCN activity increased at various stages under different SS. At a SS higher than 0.4%, N_{CCN} peaked at 20:00 LT on 3 April. N_{CCN} greatly promoted from 8000-12,000 cm^{-3} to 13,000-20,000 cm^{-3} under higher SS, however, only slightly from 6000 to 7000 cm^{-3} under lower SS (e.g. 0.2%). Larger critical dry diameter corresponding to lower SS should be the main reason. For example, the critical dry diameter for pure $(NH_4)_2SO_4$ particle was 83 nm at SS of 0.2% and was only 29 nm at SS of 1.0%. The newly formed particles rarely grew larger than 83 nm in size in this NPF event, hence less N_{CCN} enhancement was expected at SS of 0.2%. In summary, the N_{CCN} enhancement ratios were 1.17-1.88 depending on SS value. In Beijing, a larger N_{CCN} enhancement ratio of 1.4-7 was observed under SS of 0.07-0.86% caused by NPF (Yue et al., 2011).

In comparison with N_{CCN}, aerosol CCN activity was more sensitive to aerosol size spectra and meteorology factors, which exerts a big complexity into the temporal variation of aerosol activation. Aerosol activities were effectively reduced by abundant ultra-fine aerosol particles

(CCN-inert) produced during the nucleation period. The minimum (0.2-0.6) of aerosol activities was found at 13:00 LT on April when the particle growth started. Owing to the high survival probability of particles growing from nucleation mode to accumulation mode (CCN size), aerosol activities began to increase at different steps for varying SS and reached their maximums of 0.3-0.9 (0.2-1.0% SS) at 4:00 LT on 4 April, eight hours after N_{CCN} peaked.

3.2.4 Towards CCN closure for NPF

A kappa value κ describing particle hygroscopiciy, firstly introduced by Petters and Kreidenweis (2007), was employed here to get CCN closure study during NPF. Assuming aerosol particle population is totally internal-mixed, the effective integrated κ can be obtained through weighting their chemical compound volume factions,

$$\kappa = \sum_i \varepsilon_i \kappa_i \qquad (2)$$

where ε_i is the volume fraction of chemical compounds in particles, and κ_i is the effective κ of individual chemical composition. This equation has been widely used and described in detail elsewhere (Petters and and Kreidenweis., 2008; Yue et al., 2011). Aerosol particle compositions were classified into three categories, and κ_i and ε_i for individual composition are listed in Table 2, of which "others" refers to $PM_{2.5}$-(SO_4^{2-}+NO_3^-+NH_4^++Cl^-+Na^+), and is viewed as a chemical compound with κ_i=0 (Yue et al., 2011). Due to MARGA data limitations,

512 we only attempted to get CCN closure for the case NPF event in this
513 study. The hourly mean κ values were varying from 0.19 to 0.42, and had
514 an average of 0.28 during the case NPF event. In total, 83.2% of the
515 effective κ was explained by SO_4^{2-}+NO_3^-+NH_4^+, with their individual
516 contributions of 37.4%, 27.5% and 18.3%, respectively. By using the
517 calculated κ, the critical dry diameter for a particle to act as CCN at a
518 given SS can be determined from an extended κ-Köhler theory:

519 $$S(D)=\frac{D^3-D_d{}^3}{D^3-D_d{}^3(1-\kappa)}\exp\left(\frac{4\sigma_{s/a}M_\omega}{RT\rho_\omega D}\right) \quad (3)$$

520 where ρ_ω is the density of water, M_ω is the molecular weight of water,
521 $\sigma_{s/a}$ is the surface tension of the solution/air interface, *R* is the universal
522 gas constant, κ is the hygroscopicity parameter, *T* is temperature, *D* is the
523 diameter of the droplet and *S(D)* is the critical dry size under a given SS.
524 More explanation and the derivation process of equation (3) have been
525 given in detail by Petters and Kreidenweis (2007), therefore there is only
526 brief summarization here. The CCN population can be effectively viewed
527 as a subset of measured aerosol size distributions since the operating
528 range includes the majority of atmospheric particles (10-800 nm).
529 Computed for $\sigma_{s/a}$=0.072 J m^{-2} and T=298.15 K, the predicted CCN
530 number concentration can be calculated through integration between the
531 bottom and top critical dry diameters (i.e. *S(D)*).

532 Figure 10 provides correlation analysis for the hourly-averaged (N=90)
533 predicted and measured N_{CCN} at SS of 0.2-1.0%. The agreement was

534 excellent between the predicted and measured N_{CCN}, and a linear
535 regression produced a slope of 0.98 and an intercept of -150 cm^{-3}, with a
536 correlation coefficient (R^2) of 0.96. The ratio of $N_{predicted}/N_{measured}$ varied
537 between 0.83 and 1.28 with an average of 1.04.

538 ## 4. Conclusions

539 The new particle formation (NPF) events and their impacts on the
540 abundance and properties of cloud condensation nuclei (CCN) were
541 investigated using 1-month continuous measurements collected in
542 downtown Shanghai from 1 to 30 April 2012. The NPF events were
543 observed in 8 out of the 30 days, and their formation and growth rates
544 were 0.40 $cm^{-3}\ s^{-1}$ and 4.91 nm h^{-1} on average, respectively. The growth
545 rate is important in controlling the conversion of newly formed particles
546 in NPF to possible CCN, whereas the formation rate is viewed as an
547 effective factor only at higher SS (e.g. 1.0%). This is due to the small
548 critical dry diameters for particles to act as CCN under high SS
549 conditions.

550 The NPF event on 3 April 2012 showed that aerosol particle
551 enhancement in number concentration significantly relates to the length
552 of nucleation period of NPF, and aerosol particle enhancement in mass
553 concentration depends on the growth period. The nucleation period leads
554 to increased N_{CN} and reduced aerosol activity, while the increases in N_{CCN}
555 and aerosol activity occurred during the growth period. The newly

formed particles needed enough time to grow into CCN size and thus N_{CCN} had a delayed peak compared to N_{CN}.

Closure between the measured and predicted N_{CCN} is successful during the NPF event (R^2=0.96). SO_4^{2-}+NO_3^-+NH_4^+ explained the majority of the effective κ, and minimized the impact of lacking organic matter. An overestimation of 4% for N_{CCN} is probably introduced by the following uncertainties: (1) aerosol assumed to be completely internal-mixed, which is an unrealistic condition and hardly realized in real atmosphere, (2) errors introduced by κ_i for individual chemical composition, and (3) the category "others" typically includes organic carbon (OC), elemental carbon (EC), hydrophobic inorganic and other species. Among these other species there are water soluble species contributing to CCN formation. For example, OC has an effective κ value of roughly 0.1 and has been reported to be an important contributor to particle condensational growth. The reasonable closure identified in this study implies that the detailed information of particle size spectra can build an effective CCN prediction model, and size plays a dominant role in aerosol activity during NPF.

It should be noted that the contribution of NPF to CCN has not been fully characterized in this study. For example, the loss of nucleation mode particles by coagulation and the impact of atmospheric dilution and boundary layer evolution on pre-existing and newly formed CCN are

unknown. To fully determine NPF contribution to CCN, additional information on size-resolved aerosol composition, size spectra for 3 nm or smaller particles, atmospheric sink and physicochemical process will be needed.

Acknowledgements

This research is supported by the project of “China Fog-haze monitoring and its numeric forecast operational system at various scales" （2014BAC16B01）, the National Natural Science Foundation of China (41475109, 41275126, 21190053, 21177025, 21177027, 21277028, 21377029), and partly by the Research and Development Special Fund for Public Welfare Industry (Meteorology) of CMA (GYHY201006047), the Shanghai Science and Technology Commission of Shanghai Municipality (12DJ1400100, 12DZ2260200, 14XD1400600), the Jiangsu Collaborative Innovation Center for Climate Change, and Priority fields for Ph.D. Programs Foundation of Ministry of Education of China (0110071130003), and the national non-profit scientific research program for environmental protection (201409008).

Referrence

Asmi, A., Wiedensohler, A., Laj, P., Fjaeraa, A. M., Sellegri, K., Birmili, W., Weingartner, E., Baltensperger, U., Zdimal, V., Zikova, N., Putaud,

J.-P., Marinoni, A., Tunved, P., Hansson, H.-C., Fiebig, M., Kivekäs, N., Lihavainen, H., Asmi, E., Ulevivius, V., Aalto, P. P., Swietlicki, E., Kristensson, A., Mihalopoulos, N., Kalivitis, N., Kalapov, I., Kiss, G., de Leeuw, G., Henzing, B., Harrison, R. M., Beddows, D., O'Dowd, C., Jennings, S. G., Flentje, H., Weinhold, K., Meinhardt, F., Ries, L., and Kulmala, M.: Number size distributions and seasonality of submicro particles in Europe 2008-2009, Atmos. Chem. Phys., 11, 5505-5538, doi:10.5194/acp-11-5505-2011, 2011.

Benson, D. R., Yu, J. H., Markovich, A., and Lee, S. -H.: Ternary homogeneous nucleation of H_2SO_4, NH_3, and H_2O under conditions relevant to the lower troposphere, Atmos. Chem. Phys., 11, 4755-4766, doi:10.5194/acp-11-4755-2011, 2011.

Birmili, W., and Wiedensohler, A.: New particle formation in the continental boundary layer: meteorological and gas phase parameter influence, Geophys. Res. Lett., 27, 3325-3328, doi: 10.1029/1999GL011221, 2000.

Carslaw, K. S., Spracklen, D. S., Kulmala, M., Kerminen, V. –M., Sihto, S. L., and Riipinen, I.: The impact of boundary layer nucleation on global CCN, Aip. Conf. Proc., 911-915, 2007.

Cheng, T. T., Han, Z. W., Zhang, R. J., Du, H. H., Jia, X., Wang, J. J., and Yao, J. Y.: Black carbon in a continental semi-arid area of Northeast China and its possible sources of fire emission, J. Geophys. Res., 115,

622 D23204, doi: 10.1029/2009JD013523, 2010.
623 Cheng, Y., Lee, S. C., Ho, K. F., Wang, Y. Q., Cao, J. J., Chow, J. C., and
624 Watson, J. G.: Black carbon measurement in a coastal area of south
625 China, J. Geophys Res.,111, D12310, doi: 10.1029/2005JD006663,
626 2006.
627 Dal Maso, M., Kulmala, M., Lehtinen, K. E. J., and Mäkelä, J. M.:
628 Condensation and coagulation sinks and formation of nucleation mode
629 particles in coastal and boreal forest boundary layers, J. Geophys. Res.,
630 107, doi:10.1029/2001JD001053, 2002.
631 Dal Maso, M., Kulmala, M., Riipinen, I., Wagner, R., Hussein, T., Aalto,
632 P. P., and Lehtinen, K. E. J.: Formation and growth of fresh atmospheric
633 aerosols: eight years of aerosol size distribution data from SMEAR Π,
634 Hyytiala, Finland, Boreal Env. Res., 10, 323-336, 2005.
635 Dal Maso, M., Sogacheva, L., Aalto, P. P., Riipinen, I., Komppula, M.,
636 Tunved, P., Korhonen, L., Suur-Uski, V., Hirsikko, A., Kurtén, T.,
637 Kerminen, V. -M., Lihavainen, H., Viisanen, Y., Hansson, H. -C., and
638 Kulmala, M.: Aerosol size distribution measurements at four Nordic
639 field stations: identification, analysis and trajectory analysis of new
640 particle formation bursts, Tellus, 59B, 350-361, 2007.
641 Draxler, R. R., and Rolph, G. D.: HYSPLIT (Hybrid Single-Particle
642 Lagrangian Integrated Trajectory) Model access via NOAA ARL
643 READY Website (http://www.arl.noaa.gov/HYSPLIT.php), NOAA Air

644 Resources Laboratory, Silver Spring, MD, 2014.
645 Du, H. H., Kong, L. D., Cheng, T. T., Chen, J. M., Du, J. F., Li, L., Xia,
646 X., Leng. C. P., and Huang, G. H.: Insights into summertime haze
647 pollution events over Shanghai based on online water-soluble ionic
648 composition of aerosols, Atmos. Environ., 45, 5131-5137, 2011.
649 Du, J. F., Cheng, T. T., Zhang, M., Chen, J. M., He, Q. S.,Wang, X. M.,
650 Zhang, R. J., Tao, J., Huang, G. H., Li, X., and Zha, S. P.: Aerosol size
651 spectra and particle formation events at urban Shanghai in eastern China,
652 Aerosol and Air Quality Research, 12, 1362-1372, 2012.
653 Dumka, U. C., Krishna Moorthy, K., Kumar, R., Hegde, P., Sagar, R.,
654 Pant, P., Singh, N., and Suresh Babu, S.: Characteristics of aerosol black
655 carbon mass concentration over a high altitude location in the Central
656 Himalayas from multi-year measurements, Atmos. Res., 96, 510-521,
657 2010.
658 Ehn, M., Thornton, J. A., Kleist, E., Sipilä, M., Juuninen, H., Pullinen, L.,
659 Springer, M., Rubach, F., Tillmann, R., Lee, B., Lopez-Hilfiker, F.,
660 Andres, S., Acir, I-. H., Rissanen, M., Jokinen, T., Schobesberger, S.,
661 Kangasluoma, J., Kontkanen, J., Nieminen, T., Kurtén, T., Nielsen, L. B.,
662 Jørgensen, S., Kjaergaard, H. G., Canagaratna, M., Maso, M. D., Berndt,
663 T., Petäjä, T., Wahner, A., Kerminen, V. -M., Kulmala, M., Worsnop, D.
664 R., Wildt, J., and Mentel., T. F.: A large source of low-volatility
665 secondary organic aerosol, Nature, 506, 476-479, 2014.

Fuchs, N. A. and Sutugin, A. G.: High-dispersed aerosols in Topics in Current Aerosol Research, edited by: Hidy, G. M. and Brock, J. R., Pergamon, Oxford, 2, 1-60, 1971.

Gao, J., Chai, F. H., Wang, T., Wang, S. L., and Wang, W. X.: Particle number size distribution and new particle formation: New characteristics during the special pollution control period in Beijing, J. Environ. Sci., 24, 14-21, 2012.

Gaydos, T. M., Stanier, C. O., and Pandis, S. N.: Modeling of in situ ultrafine atmospheric particle formation in the eastern United States, J. Geophys. Res., 110 (D7), doi: 10.1029/2004JD004683, 2005.

Ghan, S. J., Easter, R. C., Chapman, E. G., Abdul-Razzak, H., Zhang, Y., Leung, L. R., Laulainen, N. S., Saylor, R. D., and Zaveri, R. A.: A physically based estimate of radiative forcing by anthropogenic sulfate aerosol, J. Geophys. Res., 106, 5279-5293, 2001.

Gong, Y. G., Hu, M., Cheng, Y. F., Su, H., Yue, D. L., Liu, F., Wiedensohler, A., Wang, Z. B., Kalesse, H., Liu, S., Wu, Z. J., Xiao, K. T., Mi, P. C., and Zhang, Y. H.: Competition of coagulation sink and source rate: New particle formation in the Pearl River Delta of China, Atmos. Environ., 44, 3278-3285, 2010.

Hansen, A. D. A., H. Rosen, and T. Novakov.: The aethalometer-an instrument for the real-time measurement of optical absorption by aerosol particles, Sci. Total Environ., 36, 191-196, 1984.

688 Hennigan, C. J., Westervelt, D. M., Riipinen, I., Engelhart, G. J., Lee, T.,
689 Collett, J. L., Pandis, S. N., Adams, P. J., and Robinson, A. L.: New
690 particle formation and growth in biomass burning plumes: An important
691 source of cloud condensation nuclei, Geophys. Res. Lett., 39, L09805,
692 doi: 10.1029/2012GL050930, 2012.
693 Hildebrandt, R. L., Smith, J., Riipinen, I., Barsanti, K., Fry, J., Yli-Juuti,
694 T., Petaja, T., Kulmala, M., and McMurry, P. H.: The role of nitrate in
695 the formation of atmospheric nanoparticlers: insights from ambient
696 measurements and chemical transport models, (611f) Environmental
697 division, American Institute of Chemical Engineers Annual Meeting,
698 Pittsburgh, PA, 1 November 2012, 2012.
699 Huang, Y. L., Li, L., Li, J. Y., Wang, X., Chen, H., Chen, J. M., Yang, X.,
700 Cross, D. S., Wang, H., Qiao, L. P., and Chen, H.: A case study of the
701 highly time-resolved evolution of aerosol chemical and optical
702 properties in urban Shanghai, China, Atmos. Chem. Phys., 13,
703 3931-3944, doi:10.5194/acp-13-3931-2013, 2013.
704 Hudson, J. G., and Noble, S.: CCN and vertical velocity influences on
705 droplet concentrations and supersaturations in clean and polluted stratus
706 clouds, J. Atmos. Sci., 106, 24119-24126, 2014.
707 Hussein, T., Martikainen, J., Junninen, H., Sogacheva, L., Wagner, R.,
708 Dal Maso, M., Riipinen, I., Aalto, P. P., and Kulmala, M.: Observation
709 of regional new particle formation in the urban atmosphere, Tellus B, 60,

609-521, doi:10.1111/j.1600-0889.2008.00365.x, 2008.

IPCC: Climate Change 2013: The Physical Science Basis. Contribution of Working Group I to the Fifth Assessment Report of the Intergovernmental Panel on Climate Change, edited by: Joussaume, S., Penner, J., and Tangang, F., IPCC, Stockholm, 2013.

Kerminen, V. -M.: How significantly does coagulation scavenging limit atmospheric particle production?, J. Geophys. Res., 106, 24119-24126, 2001.

Kerminen, V. -M., Lihabainen, H., Lomppula, M., Viisanen, Y., and Kulmala, M.: Direct observational evidence linking atmospheric aerosol formation and cloud droplet activation, Geophys. Res. Lett., 32, L14803, doi: 10.1029/2005GL023130, 2005.

Kerminen, V. -M., Paramonov, M., Anttila, T., Riipinen, I., Fountoukis, C., Korhonen, C., Asmi, E., Laakso, L., Lihavainen, H., Swietlicki, E., Svenningsson, B., Asmi, A., Pandis, S. N., Kulmala, M., and Petäjä, T.: Cloud condensation nuclei production associated with atmospheric nucleation: a synthesis based on existing literature and new results, Atmos. Chem. Phys., 12, 12037-12059, doi:10.5194/acp-12-12037-2012, 2012.

Köhler, H.: The nucleus in and the the growth of hygroscopic droplets, T. Faraday Soc., 32, 1152-1161, 1936.

Kristensson, A., Dal Maso, M., Swietlicki, E., Hussein, T., Zhou, J.,

732 Kerminen, V. -M, and Kulmala, M.:Characterization of new particle
733 formation events at a background site in Southern Sweden: relation to
734 air mass history, Tellus 60B, 330-344,
735 doi:10.1111/j.1600-0889.2008.00345.x, 2008.
736 Kulmala, M., Dal Maso, M., Mäkelä, J. M., Pirjola, L., Väkevä, M.,
737 Aalto, P., Miikkulainen, P., Hämeri, K., and O'Dowd, C. D.: On the
738 formation, growth and composition of nucleation mode particles, Tellus
739 B, 53, 479-490, 2001.
740 Kulmala, M., Laakso, L., Lehtinen, K. E. J., Riipinen, I., Dal Maso, M.,
741 Anttila, T., Kerminen, V. –M., Hõrrak, U., Vana, M., and Tammet, H.:
742 Initial steps of aerosol growth, Atmos. Chem. Phys., 4, 2553-2560,
743 doi:10.5194/acp-4-2553-2004, 2004.
744 Kulmala, M., Petäjä, T., Mönkkönen, P., Koponen, I. K., Dal Maso, M.,
745 Aalto, P. P., Lehtinen, K. E. J., and Kerminen, V. -M.: On the growth of
746 nucleation mode particles: source rates of condensable vapor in polluted
747 and clean environments, Atmos. Chem, Phys., 5, 409-416,
748 doi:10.5194/acp-5-409-2005, 2005.
749 Kulmala, M., Kontkanen, J., Junninen, H., Lehtipalo, K., Manninen, H. E.,
750 Nieminen, T., Petäjä, T., Sipilä, M., Schobesberger, S., Rantala, P.,
751 Franchin, A., Jokinen, T., Järvinen, E., Äijälä, M., Kangasluoma, J.,
752 Hakala, J., Aalto, P. P., Paasonen, P., Mikkilä, J., Vanhanen, J., Aalto, J.,
753 Hakola, H., Aakkonen, U., Ruuskanen, T., Mauldin III, R. L., Duplissy,

754 J., Vehkamäki, H., Bäck, J., Kortelainen, A., Riipinen, L., Kurtén, T.,
755 Johnston, M. V., Smith, J. N., Ehn, M., Mentel, T. F., Lehtinen, K. E. J.,
756 Laaksonen, A., Kerminen, V. -M., and Worsnop, D. R.: Direct
757 observations of atmospheric aerosol nucleation, Science, 339, 943-946,
758 2013.
759 Kulmala, M., Petäjä, T., Nieminen, T., Sipilä, M., Manninen, H. E.,
760 Lehtipato, K., Dal Maso, M., Aalto, P. P., Junninen, H., Paasonen, P.,
761 Riipinen, I., Lehtinen, K. E., Laaksonen, A., and Kerminen, V. -M.:
762 Measurement of the nucleation of atmospheric aerosol particles, Nat.
763 Protoc., 7, 1651–1667, 2012.
764 Kuwata, M. and Kondo, Y.: Dependence of size-resolved CCN spectra on
765 the mixing state of nonvolatile cores observed in Tokyo. J. Geophys.
766 Res., 113, D19202, doi; 10.1029/2007JD009761, 2008.
767 Laakso, L., Merikanto, J., Vakkari, V., Laakso, H., Kulmala, M., Molefe,
768 M., Kgabi, N., Mabaso, D., Carslaw, K. S., Spracklen, D. V., Lee, L. A.,
769 Reddington, C. L., and Kerminen, V. -M.: Boundary layer nucleation as
770 a source of new CCN in savannah environment, Atmos. Chem. Phys, 13,
771 1957-1972, doi:10.5194/acp-13-1957-2013, 2013.
772 Laaksonen, A., Hamed, A., Joutsensaari, J., Hiltunen, L., Cavalli, F.,
773 Junkermann, W., Asmi, A., Fuzzi, S., and Facchini, M. C.: Cloud
774 condensation nucleus production from nucleation events at a highly
775 polluted region, Geophys. Res. Lett., 32, L06812, doi;

776 10.1029/2004GL022092, 2005.
777 Lance, S., Medina, J., Smith, J. N., and Nenes, A.: Mapping the operation
778 of the DMT Continuous Flow CCN counter, Aerosol Sci. Tech., 40,
779 242-254, 2006.
780 Leng, C. P., Cheng, T. T., Chen, J. M., Zhang, R. J., Tao, J., Huang, G. H.,
781 Zha, S. P., Zhang, M. G., Fang, W., Li, X., and Li, L.: Measurements of
782 surface cloud condensation nuclei and aerosol activity in downtown
783 Shanghai, Atmos. Environ., 69, 354-361, 2013.
784 Lihavainen, H., Kerminen, V. -M., Komppula, M., Hatakka, J., Aaltonen,
785 V., Kulmala, M., and Viisanen, Y.: Production of "potential" cloud
786 condensation nuclei associated with atmospheric new particle formation
787 in north Finland, J. Geophys. Res., 108, D24, 4872, doi;
788 10.1029/2003JD003887, 2003.
789 Lohmann, U. and Feichter, J.: Global indirect aerosol effect; a review,
790 Atmos. Chem. Phys., 5, 715-737, doi:10.5194/acp-5-715-2005, 2005.
791 McMurry, P. H., Takano, H., and Anderson, G. R.: Study of the ammonia
792 (gas)-sulphuric acid (aerosol) reaction rate, Enviro. Sci. and Tech, 17,
793 347-352, 1983.
794 McMurry, P. H., Fink, M., Sakurai, H., Stolzenburg, M. R., Mauldin, R.
795 L., Smith, J., Eisele, F., Moore, K., Sjostedt, S., Tanner, D., Huey, L. G.,
796 Nowak, J. B., Edgerton, E., and Voisin, D.: A criterion for new particle
797 formation in the sulfur-rich Atlanta atmosphere, J. Geophys. Res., 110,

798 D22S02, doi; 10.1029/2005JD005907, 2005.
799 Merikanto, J., Sprackken, D. V., Mann, G. W., Pickering, S. J and Carslaw,
800 K. S.: Impact of nucleation on global CCN, Atmos. Chem. Phys., 9(21),
801 8601-8616, doi:10.5194/acp-9-8601-2009, 2009.
802 Metzger, A., Verheggen, B., Dommen, J., Duplissy, J., Prevot, A. S.,
803 Weingartner, E., Riipinen, I., Kulmala, M., Spracklen, D. V., Carslaw, K.
804 S., and Baltensperger, U.: Evidence for the role of organic in aerosol
805 particle formation under atmospheric conditions, P. Natl. Acad. Sci.
806 USA, 107, 6646-6651, 2010.
807 Mönkkönen, P., Koponen, I. K., Lehtinen, K. E. J., Hämeri, K., Uma, R.,
808 and Kulmala, M.: Measurement in a highly polluted Asian mega city:
809 observations of aerosol number size distribution, modal parameters and
810 nucleation events, Atmos. Chem. Phys., 5, 57-66,
811 doi:10.5194/acp-5-57-2005, 2005.
812 Nieminen, T., Manninen, H. E., Sihto, S. L., Yli-Juuti, T., Mauldin, R. L.,
813 Petaja, T., Riipinen, I., Kerminen, V. -M., and Kulmala, M.: Connection
814 of sulfuric acid to atmospheric nucleation in boreal forest, Environ. Sci.
815 Technol., 43, 4715-4721, 2009.
816 O'Dowd, C. D.: Biogenic coastal aerosol production and its influence on
817 aerosol radiative properties, J. Geophys Res.,106, 1545-1549, 2001.
818 O'Dowd, C. D., Aalto, P., Hameri, K., Kulmala, M., and Hoffmann, T.:
819 Atmospheric particles from organic vapors, Nature, 416, 497-498, 2002.

820 Paasonen, P., Nieminen, T., Asmi, E., Manninen, H. E., Petäjä, T.,
821 Plass-Dülmer, C., Flentje, H., Birmili, W., Wiedensaohler, A., Hõrrak, U.,
822 Metzger, A., Hamed, A., Laaksonen, A., Facchini, M. C., Kerminen, V.
823 M., and Kulmala, M.: On the role of sulphuric acid and low-volatility
824 organic vapors in the initial steps of atmospheric new particle formation,
825 Atmos. Chem. Phys., 10, 11223-11242, doi:10.5194/acp-10-11223-2010,
826 2010.
827 Petäjä, T., Mauldin, R. L., Kosciuch, E., ,McGrath, J., Nieminen, T.,
828 Passonen, P., Boy, M., Adamov, A., Kotiaho, T., and Kulmala, M.:
829 Sulfuric acid and OH concentrations in a boreal forest site, Atmos.
830 Chem. Phys., 9, 7435-7448, doi: 10.5194/acp-9-7435-2009, 2009.
831 Petters, M. D., and Kreidenweis, S. M.: A single parameter representation
832 of hygroscopic growth and cloud condensation nucleus activity, Atmos.
833 Chem. Phys., 7, 1961-1971, doi:10.5194/acp-7-1961-2007, 2007.
834 Petzold, A., Kopp, C., and Niessner, R.: The dependence of the specific
835 attenuation cross-section on black carbon mass fraction and particle size,
836 Atmos. Environ., 31, 661-672, 1997.
837 Pierce, J. R., and Adams, P. J.: Efficiency of cloud condensation nuclei
838 formation from ultrafine particles, Atmos. Chem. Phys., 7, 1367-1379,
839 doi:10.5194/acp-7-1367-2007, 2007.
840 Pierce, J. R., and Adams, P. J.: Uncertainty in global CCN concentrations
841 from uncertain aerosol nucleation and primary emission rates, Atmos.

842 Chem. Phys., 9, 1339-1356, doi:10.5194/acp-9-1339-2009, 2009.
843 Ramanathan, V., Crutzen, P. J., Kiehl, J. T., and Rosenfeld, D.: Aerosols,
844 Climate, and the Hydrological Cycle, Science, 294, 2119-2124, 2001.
845 Riipinen, I., Pierce, J. R., Yli-Juuti, T., Nieminen, T., Häkkinen, S., Ehn,
846 M., Junnunen, H., Lehtipalo, K., Petäjä, T., Slowlk, J., Chang, R.,
847 Shantz, N. C., Abbatt, J., Leaitch, W. R., Kerminen, V. –M., Worsnop, D.
848 R., Pandis, S. N., Donahue, N. M., and Kulmala, M.: Organic
849 condensation: a vital link connecting aerosol formation to cloud
850 condensation nuclei (CCN) concentrations, Atmos. Chem. Phys., 11,
851 3865-3878, doi:10.5194/acp-11-3865-2011, 2011.
852 Roberts, G. C. and Nenes, A.: A continuous-flow streamwise
853 thermal-gradient CCN chamber for atmospheric measurements, Aerosol
854 Sci. Tech., 39, 206-221, 2006.
855 Sakurai, T., Fujita, S. I., Hayami, H., and Furuhashi, N.: A study of
856 atmospheric ammonia by means of modeling analysis in the Kanto
857 region of Japan, Atmos. Environ., 39, 203-210, 2005.
858 Shen, X. J., Sun, J. Y., Zhang, Y. M., Wehner, B., Nowak, A., Tuch, T.,
859 Zhang, X. C., Wang, T. T., Zhou, H. G., Zhang, X. L., Dong, F., Birmili,
860 W., and Wiedensohler, A.: First long-term study of particle number size
861 distributions and new particle formation events of regional aerosol in the
862 North China Plain, Atmos. Chem. Phys., 11, 1565-1580,
863 doi:10.5194/acp-11-1565-2011, 2011.

Smith, J. N., Moore, K. F., McMurry, P. H., and Eisele F. L.: Atmospheric measurements of sub-20 nm diameter particle chemical composition by thermal desorption chemical ionization mass spectrometry, Aerosol Sci. Technol, 38, 100-110, 2004.

Spracklen, D. V., Carslaw, K. S., Kulmala, M., Kerminen, V. M., Mann, G. W., and Sihto, S. L.: The contribution of boundary layer nucleation events to total particle concentrations on regional and global scales, Atmos. Chem. Phys., 6, 5631-5648, doi:10.5194-acp-6-5631-2006, 2006.

Spracklen, D. V., Carslaw, K. S., Kulmala, M., Kerminen, V. M., Sihto, S. L., Riipinen, I., Merikanto, J., Mann, g. w., Chipperfield, M. P., Wiedensohler, A., Birmili, W., and Lihavainen, H.: Contribution of particle formation to global cloud condensation nuclei concentrations, Geophys. Res. Lett., 35, L06808, doi:10.1029/2007GL033038, 2008.

Vehkamäki, H., Dal Maso, M., Hussein, T., Flannagan, R., Hyvärinen, A., Lauros, J., Merikanto, J., Mönkkönen, P., Pihlatie, M., Salminen, K., Sogacheva, L., Thum, T., Ruuskanen, T. M., Keronen, P., Aalto, P. P., Hari, P., Lehtinen, K. E. J., Rannik, Ü., and Kulmala, M.: Atmospheric particle formation events at Värriö measurement station in Finnish Lapland 1998-2002, Atmos. Chem. Phys., 4, 2015-2023, doi:10.5194/acp-4-2015-2004, 2004.

Vuollekoski, H., Kerminen, V. -M., Anttila, T., Sihto, S. L., Vana, M., Ehn,

M., Korhonen, H., McFiggans, G., O'Dowd, C. D., and Kulmala, M.: Iodine dioxide nucleation simulations in coastal and remote marine environments, J. Geophys. Res., 114, D00206, doi: 10.1029/2008JD010713, 2009.

Wang, X. F., Zhang, Y. P., Chen, H., Yang, X., and Chen, J. M.: Particle nitrate formation in a highly polluted urban area: a case study by single-particle mass spectrometry in Shanghai, Environ. Sci. Technol., 43, 3061-3066, 2009.

Wang, Y., Zhuang, G. S., Zhang, X. Y., Huang, K., Xu, C., Tang, A. H., Chen, J. M., and An, Z. S.: The ion chemistry, seasonal cycle, and sources of $PM_{2.5}$ TSP aerosol in Shanghai, Atmos. Enviro.,40, 2935-2952, 2006.

Wang, Z. B., Hu, M., Sun, J. Y., Wu, Z. J., Yue, D. L., Shen, X. J., Zhang, Y. M., Pei, X. Y., Cheng, Y. F., and Wiedensohler, A.: Characteristics of regional new particle formation in urban and regional background environments in the North China Plain, Atmos. Chem. Phys., 13, 12495-12506, 3013.

Wang, Z. B., Hu, M., Wu, Z. J., and Yue, D. L., Reaserch on the formation mechanism of new particles in the atmosphere, Acta Chim. Sinica, 71, 519-527, 2013.

Weber, R. J., Marti, J. J., McMurry, P. H., Eisele, F. L., Tanner, D. J., and Jefferson, A.: Measured atmospheric new particle formation rates:

908 Implications for nucleation mechanisms, Chem. Eng. Commun., 151,
909 53-64, 1996.
910 Weber, R. J., McMurry, P. H., Mauldin, R. L., Tanner, D. J., Eisele, F. L.,
911 Clarke, A. D., and Kapustin, V. N.: New particle formation in the remote
912 troposphere: a comparison of observations at various sites, Geophys.
913 Res. Lett., 26, 307-310, doi:10.1029/1998GL900308, 1999.
914 Weingartner, E., Saathoff, H., Schnaiter, M., Streit, N., Bitnar, B., and
915 Baltensperger, U.: Absorption of light by soot particles: determination of
916 the absorption coefficient by means of aethalometers, J. Aerosol Sci., 34,
917 1445-1463, 2003.
918 Wiedensohler, A., Cheng, Y. F., Nowak, A., Wehner. B., Achtert, P.,
919 Berghof, M., Birmili, W., Wu, Z. J., Hu, M., Zhu, T., Takegawa, N., Kita,
920 K., Kondo, Y., Lou, S. R., Hofzumahaus, A., Holland, F., Wahner, A.,
921 Gunthe, S. S., Rose, D., Su, H., and Pöschl. U.: Rapid aerosol growth
922 and increase of cloud condensation nucleus activity by secondary
923 aerosol formation and condensation: a case study for regional air
924 pollution in northeastern China, Geophys. Res. Lett., 114, D00G08,
925 doi:10.1029/2008JD010884, 2009
926 Wu, Z., Hu, M., Liu, S., Wehner, B., Bauer, S., Mäßling, A.Wiedensohler,
927 A., Petäjä, T., Dal Maso, M., and Kulmala, M.: New particle formation
928 in Beijing, China: statistical analysis of a 1-year dataset, J. Geophys.
929 Res., 112, D09209, doi; 10.1029/2006JD007406, 2007.

930 Wu, Z. J., Hu, M., Lin, P., Liu, S., Wehner, B., and Wiedensohler, A.:
931 Particle number size distribution in the urban atmosphere of Beijing,
932 China, Atmos. Environ., 42, 7967-7980,
933 doi:10.1016/j.atmosenv.2008.06.022, 2008.
934 Yu, F. Q.: Effect of ammonia on new particle formation: a kinetic
935 H_2SO_4-H_2O-NH_3 nucleation model constrained by laboratory
936 measurements, J. Geophys. Res., 111, D01204, doi;
937 10.1029/2005JD005968, 2006.
938 Yu, F., Wang, Z., Luo, G., and Turco, R.: Ion-mediated nucleation as an
939 important global source of tropospheric aerosols, Atmos. Chem. Phys., 8,
940 2537-2554, doi:10.5194/acp-8-2537-2008, 2008.
941 Yu, H., McGraw, R., and Lee, S. H.: Effects of amines on formation of
942 sub-3 nm particles and their subsequent growth, Geophys. Res. Lett., 39,
943 L02807, doi: 10.1029/2011GL050099, 2012.
944 Yue. D. L., Hu. M., Zhang. R. J., Wu. Z. J., Su. H., Wang, Z. B., Peng, J.
945 F., He, L. Y., Huang, X. F., Gong, Y. G., and Wiedensohler, A.: Potential
946 contribution of new particle formation to cloud condensation nuclei in
947 Beijing, Atmos. Environ., 45, 6070-6077, 2011.
948 Zhang, R. J., Jing, J. S., Tao, J., Hsu, S.-C., Wang, G., Cao, J. J., Lee, C. S.
949 L., Zhu, L., Chen, Z., Zhao, Y., and Shen, Z.: Chemical characterization
950 and source apportionment of $PM_{2.5}$ in Beijing: seasonal perspective,
951 Atmos. Chem. Phys., 13, 7053-7074, doi:10.5194/acp-13-7053-2013,

2013.

Zhang, R. Y.: Getting to the critical nucleus of aerosol formation, Science, 328, 1366-1367, 2010.

Zhang, R. Y., Khalizov, A., Wang, L., Hu, M., and Xu, W.: Nucleation and growth of nanoparticles in the atmosphere, Chem. Rev., 112, 1957-2011, 2012.

Zheng, J., Hu, M., Zhang, R., Yue, D., Wang, Z., Guo, S., Li, X., Bohn, B., Shao, M., He, L., Huang, X., Wiedensohler, A., and Zhu, T.: Measurements of gaseous H_2SO_4 by AP-ID-CIMS during CAREBijng 2008 Campaign, Atmos. Chem. Phys., 11, 7755-7765, doi:10.5194/acp-11-7755-2011, 2011.

974 **Table 1.** Comparison of CCN enhancement ratios from NPF events with
975 different formation and growth rates.

	0.2%	0.4%	0.6%	0.8%	1.0%
Enhancement ratio (FR>0.40)	1.18	1.84	1.88	1.84	1.77
Enhancement ratio (FR<0.40)	1.15	1.89	1.81	1.77	1.58
Enhancement ratio (GR>4.91)	1.25	1.95	2.03	1.93	1.72
Enhancement ratio (GR<4.91)	1.10	1.79	1.80	1.74	1.63

976

977 **Table 2.** Effective hygroscopicity parameters (κ) and densities of the four
978 category compositions.

Species	Data source	κ	Density (g cm^{-3})
Sulfate & nitrate	SO_4^{2-}+NO_3^-+NH_4^+	0.6	1.7
Sodium chloride	Cl^-+Na^+	1	2.2
Insoluble compounds	Others	0	2.0

979

980 **Figure captions**

981 **Figure 1**. Series of 10-min mean meteorological parameters over the
982 entire campaign.

983 **Figure 2.** Series of 5-min mean SO_2 and $PM_{2.5}$ concentration and
984 atmospheric visibility over the entire campaign.

985 **Figure 3.** Series of aerosol size distribution, 4-min mean total (N_{total}) and
986 nucleation ($N_{10\text{-}20nm}$) mode aerosol number concentration and 1-hour
987 mean CCN concentration over the entire campaign.

Figure 4. Temporal evolution of 4-min mean aerosol size spectra, showing new particle formation and subsequent growth on 3 and 4 April 2012.

Figure 5. Temporal evolution of 10-min mean meteorological parameters during the new particle formation event on 3-4 April 2012.

Figure 6. Temporal evolutions of 5-min mean atmospheric visibility, BC and $PM_{2.5}$ concentrations during the new particle formation event on 3-4 April 2012.

Figure 7. Temporal evolutions of 4-min mean mode, median and diameters and 10-20 nm particle concentration, showing the growth rate and formation of new particle on 3-4 April 20.

Figure 8. Series of 1-h mean SO_2, SO_4^{2-}, NO_3^- and NH_4^+ concentrations on 3 and 4 April 2012.

Figure 9. Series of 1-h mean CCN concentration and CCN/CN on 3 and 4 April 2012.

Figure 10. Scatterplots of predicted and measured CCN concentrations (cm^{-3}) at different *SS* conditions, the red dash line represents y=x.

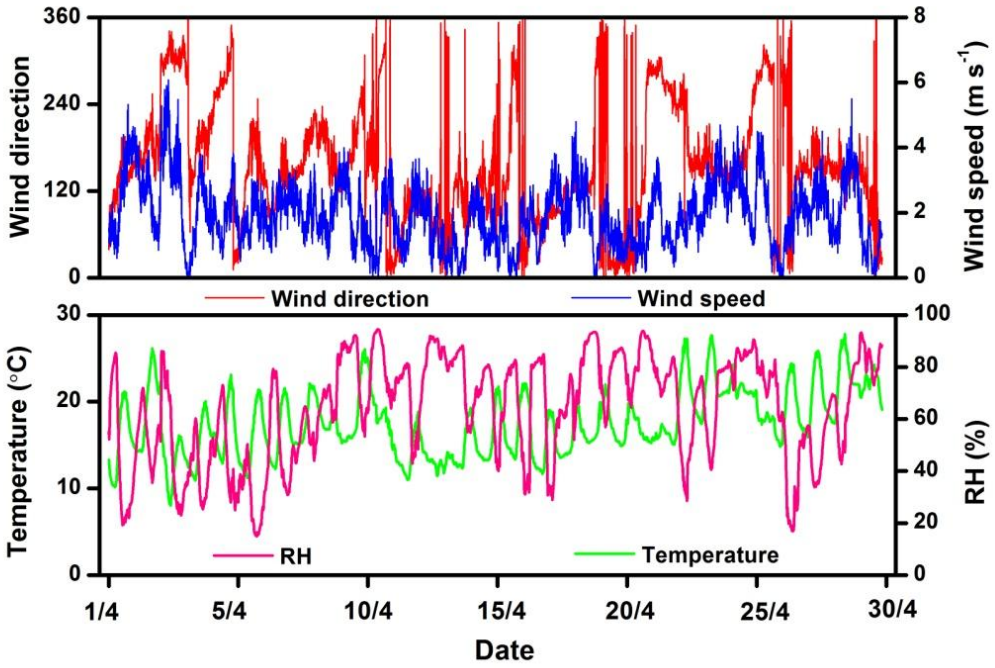

Figure 1. Series of 10-min mean meteorological parameters over the entire campaign.

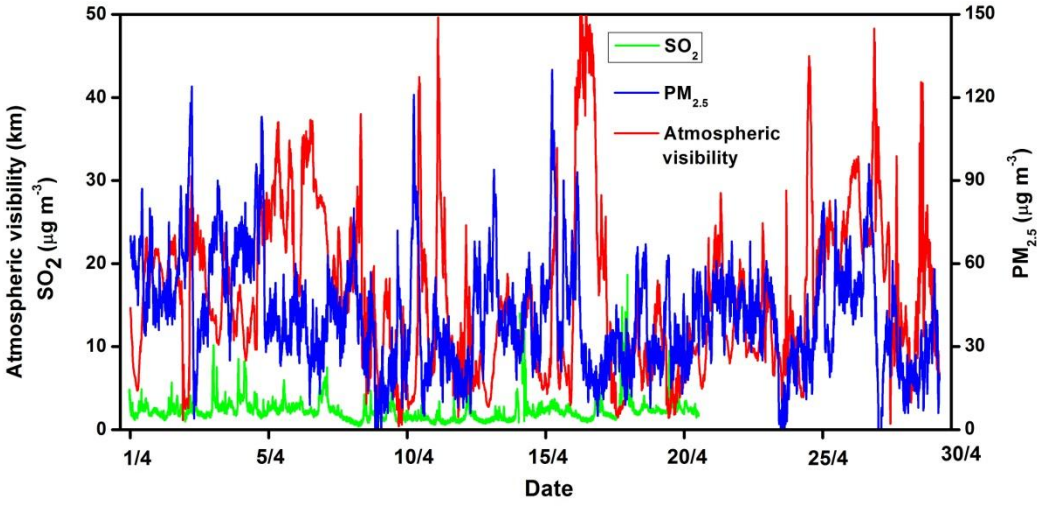

Figure 2. Series of 5-min mean SO_2 and $PM_{2.5}$ concentration and atmospheric visibility over the entire campaign.

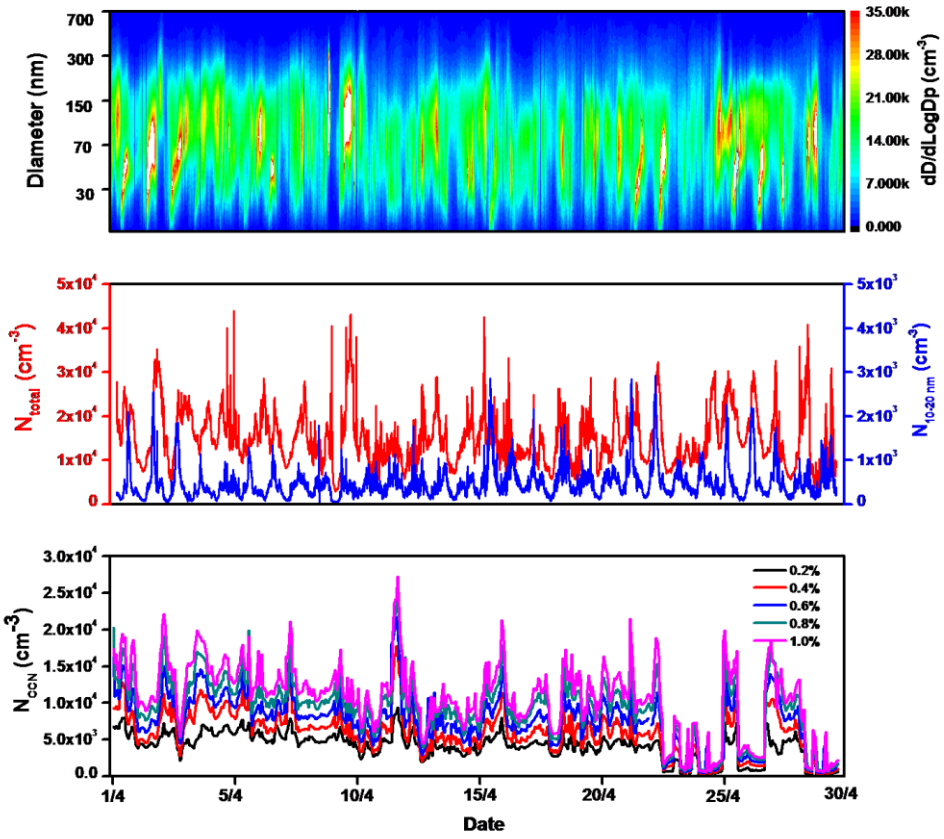

Figure 3. Series of aerosol size distribution, 4-min mean total (N_{total}) and nucleation ($N_{10\text{-}20nm}$) mode aerosol number concentration and 1-hour mean CCN concentration over the entire campaign.

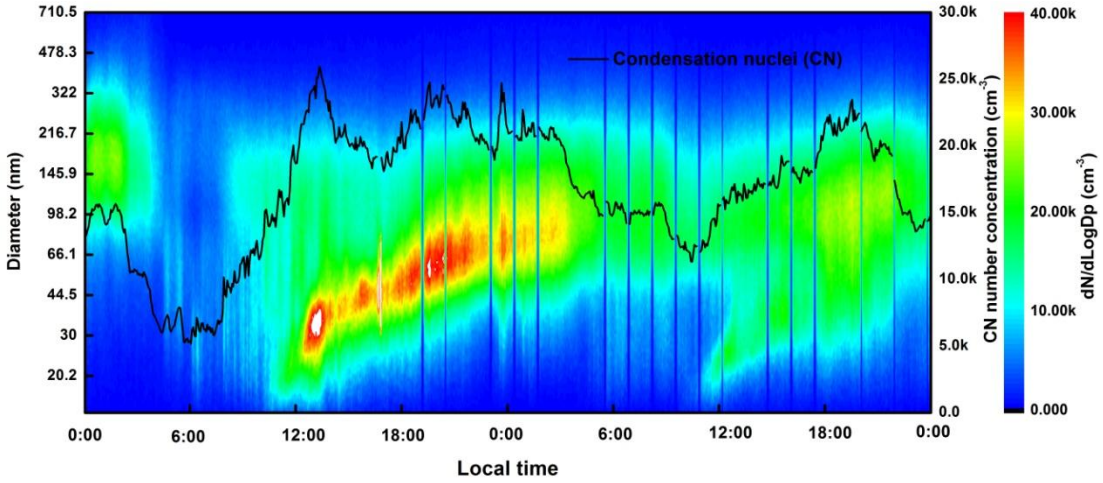

Figure 4. Temporal evolution of 4-min mean aerosol size spectra, showing new particle formation and subsequent growth on 3 and 4 April 2012.

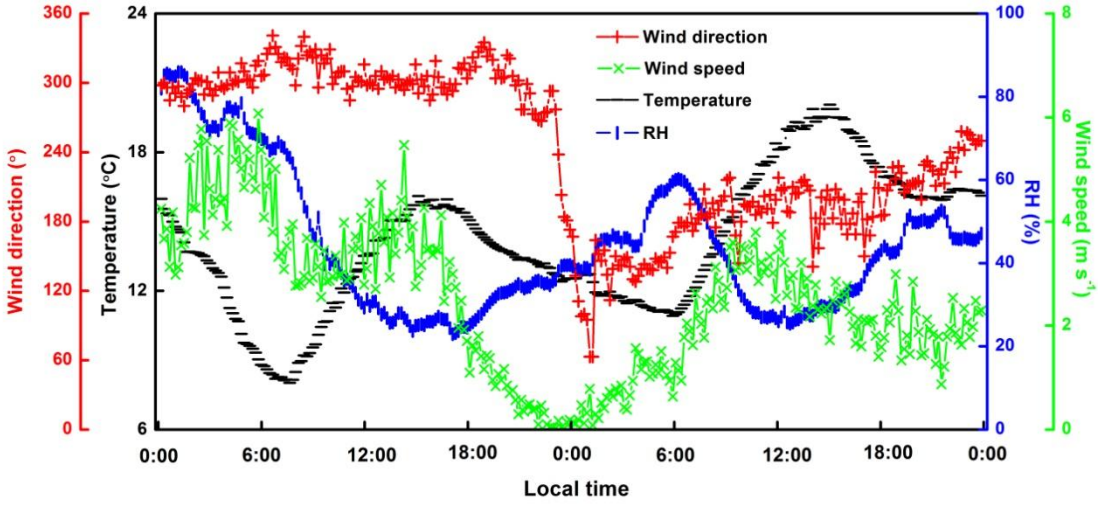

Figure 5. Temporal evolution of 10-min mean meteorological parameters during the new particle formation event on 3-4 April 2012.

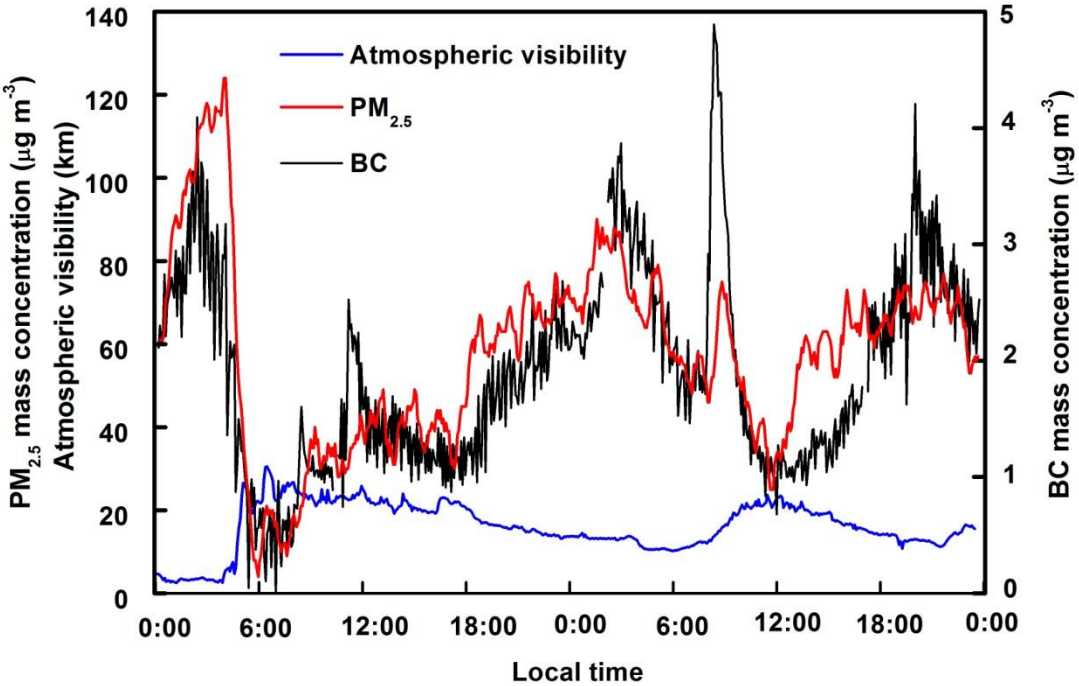

Figure 6. Temporal evolutions of 5-min mean atmospheric visibility, BC and $PM_{2.5}$ concentrations during the new particle formation event on 3-4 April 2012.

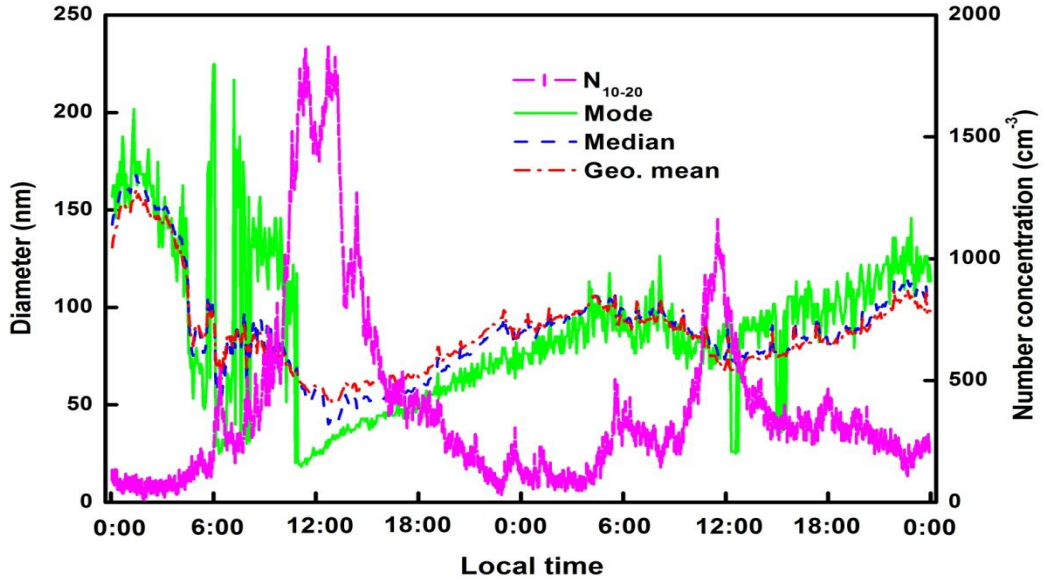

Figure 7. Temporal evolutions of 4-min mean mode, median and diameters and 10-20 nm particle concentration, showing the growth rate and formation of new particle on 3-4 April 20.

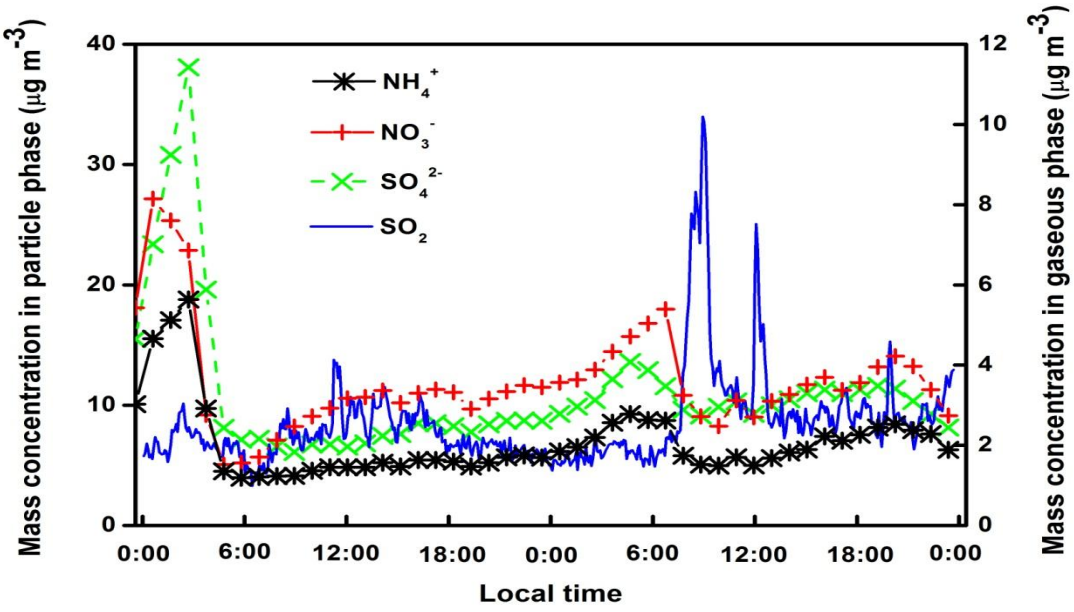

Figure 8. Series of 1-h mean SO_2, SO_4^{2-}, NO_3^- and NH_4^+ concentrations on 3 and 4 April 2012.

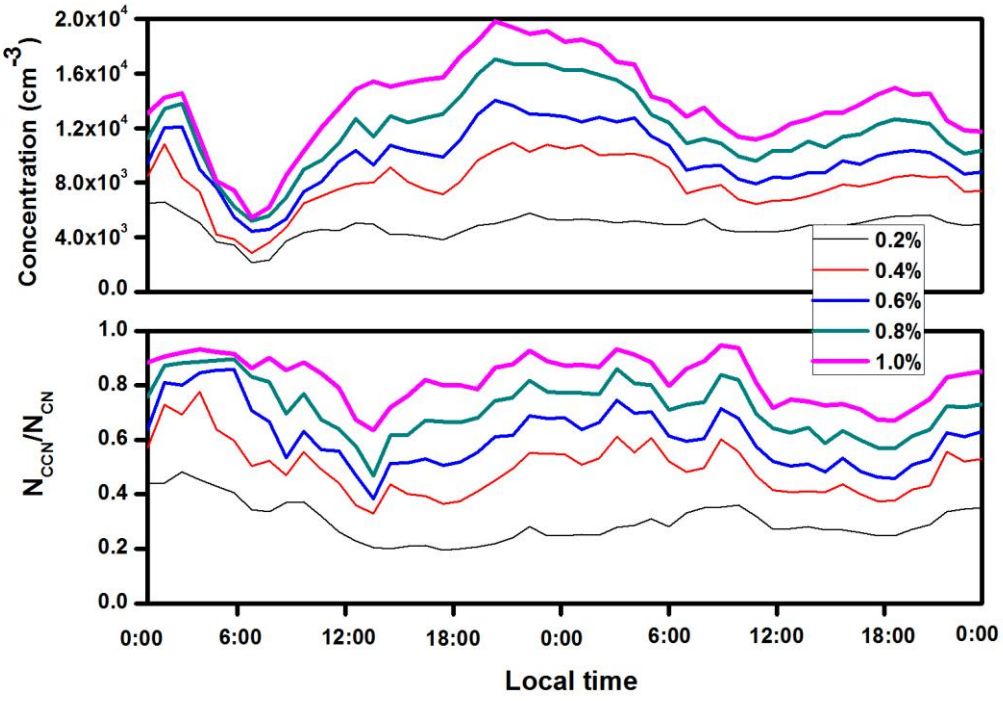

Figure 9. Series of 1-h mean CCN concentration and CCN/CN on 3 and 4 April 2012.

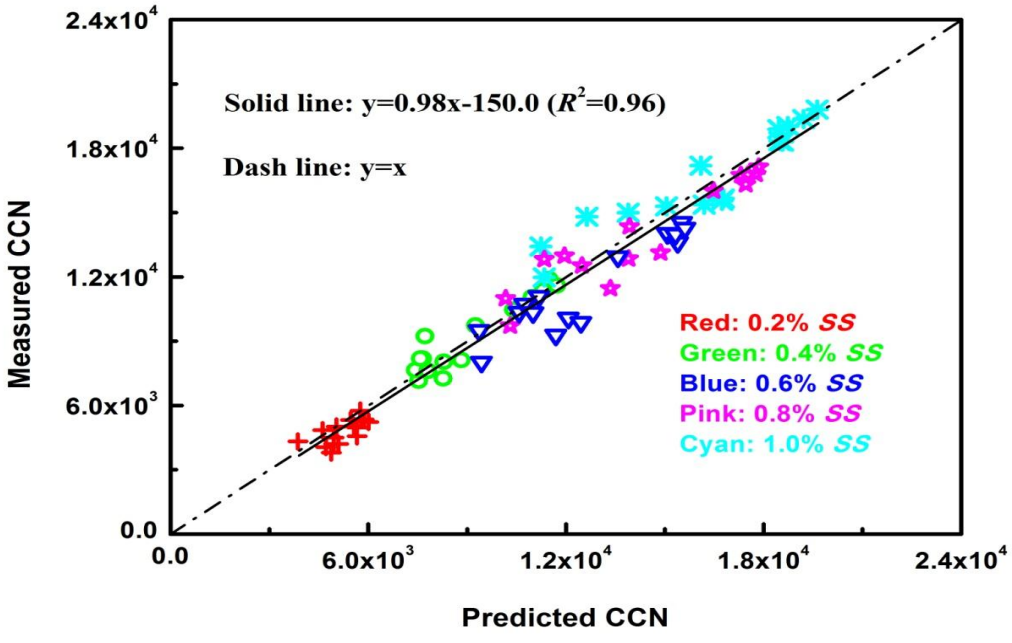

Figure 10. Scatterplots of predicted and measured CCN concentrations (cm^{-3}) at different *SS* conditions, the red dash line represents y=x.